Proceedings of ASME-JSME-KSME Joint Fluids Engineering Conference 2011
AJK2011-FED
July 24-29, 2011, Hamamatsu, Shizuoka, JAPAN

AJK2011-25020

SPATIO-TEMPORAL CHARACTERISTICS OF HEAT TRANSFER IN SEPARATED AND REATTACHING FLOWS

Hajime Nakamura
National Defense Academy
Yokosuka, Kanagawa, Japan

Sayaka Takaki
National Defense Academy
Yokosuka, Kanagawa, Japan

Shunsuke Yamada
National Defense Academy
Yokosuka, Kanagawa, Japan

ABSTRACT

Spatio-temporal characteristic of heat transfer accompanied by the flow separation and reattachment was investigated using a high-speed infrared thermograph that recorded the temperature fluctuation on a heated thin-foil. In this study, the heat transfers behind a backward-facing step, behind a forward-facing step, and on a blunt plate were investigated. In all configurations, the heat transfer in the flow reattaching region had spot-like characteristics, which spread with time and overlapped with others to form a complex feature in terms of spatio-temporal characteristics of the heat transfer. The mean Nusselt number distribution behind the reattaching region was approximately proportional to 2/3 power of Reynolds number, as indicated in the previous researches. The time-space distribution of the heat transfer had a typical spanwise wavelength and fluctuating frequency in the reattaching region, which was likely to be related to the dimension of the separation region (characteristic length H or the separation length x_R). This suggests that the origin of these periodicities is not the instability upstream of the flow separation, but due to some instability, which is accompanied by the flow separation and reattachment.

INTRODUCTION

Despite a large number of studies have been performed on the heat transfer for the separated and reattaching flow (Vogel and Eaton [1], among others), little is known so far on spatio-temporal feature of the heat transfer. This largely results from difficulties with measurements, since conventional test surfaces are difficult to respond high-frequency fluctuation of temperature accompanied with flow turbulence.

Kawamura et al. [2, 3] employed many heat flux sensors (under a condition of steady wall temperature) arranged in streamwise or spanwise directions to investigate instantaneous distributions of the heat transfer and its unsteady characteristics behind a backward facing step. Although the existence of time and spanwise periodicity in the instantaneous distribution is suggested to exist in the reattaching region, the understanding of the whole feature seems to be insufficient due to the limited space resolution of the measurement.

Hetsroni et al. [4] and Oyakawa et al. [5] employed infrared thermography to investigate surface heat transfer distribution and its fluctuating pattern behind a two-dimensional obstacle. The test surface was fabricated from a heated thin-foil, the temperature of which fluctuated according to flow turbulence. As a result, the spatio-temporal feature of the heat transfer which was reflected by the vortical structure near the surface was observed. However, there was a considerable attenuation in time and space due to the thermal inertia and the lateral conduction.

The recent improvement of infrared thermograph with respect to temporal, spatial and temperature resolutions enable us to investigate more detailed behavior of the heat transfer caused by flow turbulence. The present author (Nakamura [6]) indicated analytically that the spatio-temporal distribution of the heat transfer to air caused by flow turbulence can be investigated by employing modern infrared thermograph which measures temperature fluctuation on a heated thin-foil of sufficiently low heat capacity. The applicability of this technique was demonstrated experimentally by measuring the heat transfer on the wall of a turbulent boundary layer (Nakamura [7]). The result showed that the statistical values, that is, rms value of the fluctuating heat transfer coefficient and mean spacing of the thermal streaks, reasonably agreed to those of previous data of DNS and experiments.

In this work, this technique was applied to explore the spatio-temporal characteristics of the heat transfer accompanied by the flow separation and reattachment. The heat transfer for three representative flow fields, that is, the heat transfer behind a backward-facing step, behind a forward-facing step, and on a blunt plate, were examined. The attenuation due to both the thermal inertia and the lateral conduction of the test surface was restored by solving the heat conduction equations inside the surface. Special attention was devoted to investigate the

spatio and temporal characteristics of the heat transfer in the flow reattaching region.

NOMENCLATURE

AR	aspect ratio
b, b_c	spatial wavelength, cut-off wavelength
b_{min}	lower limit of spatial wavelength detectable
c	specific heat
d	displacement
FR	frame rate
f, f_c	fluctuating frequency, cut-off frequency
f_{max}	upper limit of fluctuating frequency detectable
H	characteristic length
h	heat transfer coefficient
l_z	mean spanwise wavelength
Nu	Nusselt number; $Nu_H = \bar{h}H/\lambda$
$P(f)$	power spectrum
$\dot{q}$	heat flux
$R(t)$	auto-correlation function
Re	Reynolds number; $Re_H = u_0 H/\nu$
St	Strouhal number; $St_H = fH/u_0$
T	temperature
T_0, T_w	freestream and wall temperatures
ΔT_{IR0}	noise equivalent temperature difference of infrared thermograph for a blackbody
t	time
u_0	freestream velocity
x, y, z	streamwise, vertical, and spanwise coordinates
x_R	flow reattachment point
x_R'	streamwise position of maximum heat transfer
δ	thickness
δ_a	thickness of air-layer
ε_t, ε_{IR}	total emissivity, spectral emissivity for infrared thermograph
λ	thermal conductivity
ν	kinematic viscosity of fluid
ρ	density

Subscript

a, c	air layer, copper plate
cd, cv	conduction, convection
$hmax$	location of maximum heat transfer coefficient
rd, rdi	radiation to outside, radiation to inside

Other symbols

$(\bar{\ })$	mean value
$\Delta(\ )$, $(\ )_{rms}$	spatial or temporal amplitude, root-mean-square value

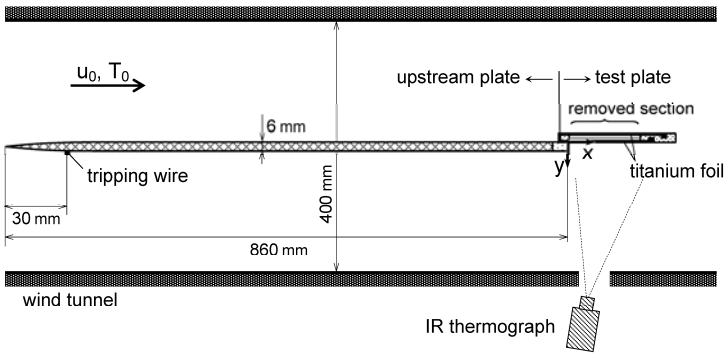

(a) Cross-sectional view of the wind tunnel

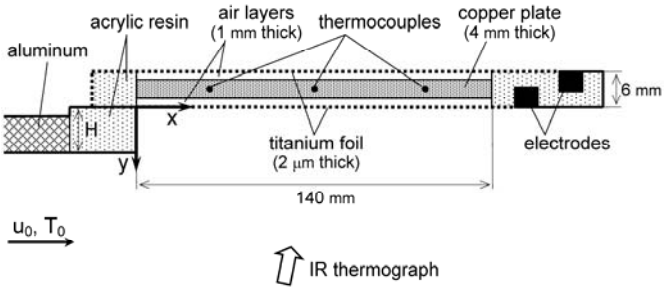

(b) Cross sectional view of the test surface (backward-facing step)

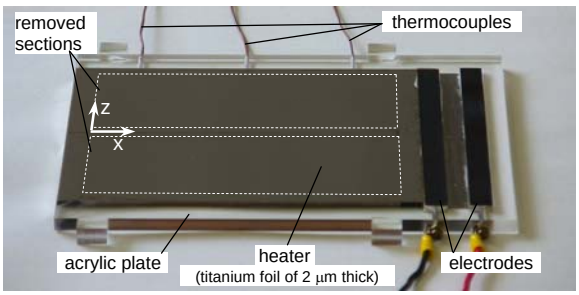

(c) Photograph of the test surface

FIGURE 1. EXPERIMENTAL SETUP

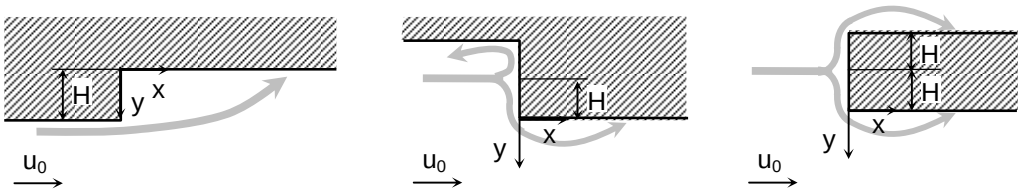

(a) Backward-facing step (BS) (b) Forward-facing step (FS) (c) Blunt plate (BP)

FIGURE 2. FLOW CONFIGURATIONS

TABLE 1. EXPERIMENTAL CONDITIONS

	H (mm)	AR (W/H)	u_0 (m/s)	Re_H	Wide measurements			Close-up measurements		
					FR (Hz)	f_c (Hz)	b_c (mm)	FR (Hz)	f_c (Hz)	b_c (mm)
BS	5	30	2 – 6	590 – 1780	420	52.5	5.3	800	200	2.2
	10	15		1180 – 3560			5.3		200	2.4
	15	10		1760 – 5330			5.3		200	2.2
FS	7.5	20		890 – 2660			5.4	1000	250	2.2
BP	3	50		350 – 1050			5.3		250	2.2

EXPERIMENTAL APPARATUS

The measurements were performed using a wind tunnel of 400 mm high × 150 mm wide (W) × 1070 mm long, as shown in Fig. 1 (a). The freestream velocity ranged u_0 = 2 – 6 m/s, the turbulent intensity in this range was about 0.5 %. Figure 2 shows the coordinate system and symbols for three flow fields, a backward-facing step (BS), a forward-facing step (FS), and a blunt plate (BP).

For the measurements of BS and FS, a turbulent boundary layer was formed on the lower-side face of a flat plate (aluminum plate) of 840 mm long, as shown in Fig. 1 (a). The momentum thickness of the turbulent boundary layer just upstream of the rear edge was 3.0 – 2.7 mm, and the wall-friction velocity and the wall-friction length were respectively $u_\tau = \sqrt{\nu\,|\partial\overline{u}/\partial y|}$ = 0.14 – 0.25 m/s and $l_\tau = \nu/u_\tau$ = 0.13 – 0.07 mm for the freestream velocity of u_0 = 3 – 6 m/s, respectively. A test plate, as shown in Fig. 1 (b) and (c), was positioned at the downstream edge of the aluminum plate to form a vertical step (BS or FS). For the measurement of BP, the aluminum plate was removed to make a uniform flow upstream of the blunt test plate. The characteristic length H for BS was defined as a step height, and that for FS and BP was defined as a length from the front stagnation point to the edge where the flow separates, as shown in Fig. 2. Here, the value of H for FS was defined as a half the step height, on the basis of the flow visualization of Igarashi et al. [8]. The experimental conditions are summarized in Table 1.

The test plate fabricated from acrylic resin (6 mm thick) had two removed sections, which were covered with a titanium foil of 2 μm thick on both the lower and upper faces (see Fig. 1 (c)). Both ends of the foil were closely adhered to electrodes

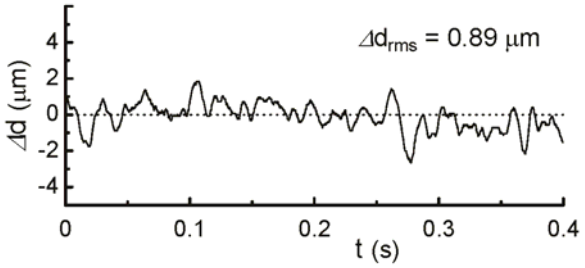

FIGURE 3. TIME TRACE OF VERTICAL DISPLACEMENT OF THE TITANIUM FOIL DUE TO MECHANICAL VIBRATION (BS: H = 10 mm at u_0 = 6 m/s, $x \approx 50$ mm, $z \approx 30$ mm)

with high-conductivity bond to suppress a contact resistance. A copper plate of 4 mm thick was placed at the mid-height of the removed section (see Fig. 1 (b)) in order to impose a boundary condition of a steady and uniform temperature. On the surface of the copper plate, a gold leaf (0.1 μm thick) was glued to suppress the thermal radiation. The titanium foil was heated by applying a direct current under conditions of constant heat flux so that the temperature difference between the foil and the freestream was about 20–30°C. Since both the upper and lower faces of the test plate were simultaneously heated, the heat conduction loss to inside the plate was much reduced. Under these conditions, air enclosed by both the titanium foil and the copper plate (1 mm thick) does not convect because the Rayleigh number is lower than 10, which is below the critical value Ra_{cr}=1708 [9].

To suppress a deformation of the heated thin-foil due to the thermal expansion of air inside the plate, thin relief holes were

connected from the ail-layer to the atmosphere. Also, the titanium foil was stretched by heating it since the thermal expansion coefficient of the titanium is smaller than that of the acrylic resin. This suppressed mechanical vibration of the foil against the flow fluctuation. Figure 3 shows an example of the vertical displacement of the foil Δd due to mechanical vibration, which was measured using a laser displacement meter (LK-G150, Keyence) at the flow reattaching region of BS at u_0 = 6 m/s (H = 10 mm, $x \approx 50$ mm, $z \approx 30$ mm). The rms value of the displacement Δd_{rms} in this condition was about 1 μm, which was one or two orders lower than the wall-friction length of the turbulent boundary layer just upstream of the step.

The infrared thermograph was positioned below the plate and it measured the fluctuation of the temperature distribution on the lower-side face of the plate through a hole on the lower wall of the wind tunnel. In this study, a high-speed infrared thermograph of SC4000, FLIR (420 frames per second with a resolution of 320×256 pixels, integration time 0.961 ms; the frame rate increases up to 1000 Hz with a reduction of the pixels number) was employed. The value of NETD (noise equivalent temperature difference) was ΔT_{IR0} = 0.018°C at the room temperature.

The temperature of the titanium foil, T_w, was determined using the following equation.

$$E_{IR} = \varepsilon_{IR} f(T_w) + (1 - \varepsilon_{IR}) f(T_a) \qquad (1)$$

where E_{IR} is the spectral emissive power detected by the infrared thermograph, $f(T)$ is the calibration function of the infrared thermograph for a blackbody (Here, $f(T)$ was expressed by a cubic equation), ε_{IR} is spectral emissivity for the infrared thermograph, and T_a is the ambient wall temperature. The first and second terms in the right side of Eq.(1) represent the emissive power from the test surface and surroundings, respectively. In order to suppress the diffuse reflection, the inner surface of the wind tunnel (the surrounding surface of the test surface) was coated with black paint. Also, in order to keep the second term to be constant, careful attention was paid to keep the surrounding wall temperature to be uniform. The thermograph was set with an inclination angle of 20° against the test surface in order to avoid the reflection of infrared radiation emitted from the thermograph itself.

The spectral emissivity of the foil, ε_{IR}, was estimated using the titanium foil, which was adhered closely to a heated copper plate. The value of ε_{IR} can be calculated from Eq.(1) by substituting E_{IR} detected by the infrared thermograph, the temperature of the copper plate ($\approx T_w$) measured using such as thermocouples, and the ambient wall temperature T_a.

The accuracy of this measurement was verified to measure the distribution of mean heat transfer coefficient of a laminar boundary layer. The result was compared to a 2D heat conduction analysis assuming the velocity distribution to be a theoretical value. The agreement was very well (within 3 %), indicating that the present measurement is reliable to evaluate the heat transfer coefficient at least for a steady flow condition (Nakamura [7]).

Also, a dynamic response of this measurement was investigated against a stepwise change of the heat input to the foil in conditions of a steady flow for a laminar boundary layer. The response curve of the measured temperature agreed well to that of the numerical analysis of the heat conduction equation (shown in Eq. (2) and (3)). This indicates that the delay due to the heat capacity of the foil, $c\rho\delta(\partial T_w/\partial t)$ in Eq.(2), and the heat conduction loss to the air-layer, $\dot{q}_{cd} = -\lambda_a (\partial T/\partial y)_{y=0-}$ in Eq.(2), can be evaluated with a sufficient accuracy (Nakamura [7]).

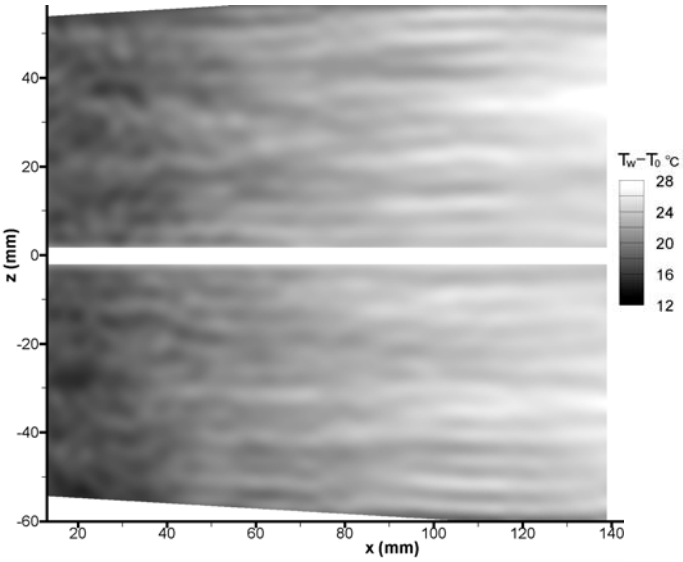

(a) Wide measurement (420Hz, 320×256 pixels)

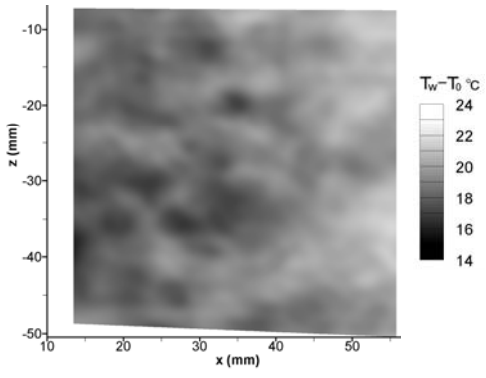

(b) Close-up measurement (1000Hz, 160×168 pixels)

FIGURE 4. TEMPERATURE DISTRIBUTION ON THE TITANIUM FOIL BEHIND THE BACKWARD-FACING STEP (FS: H = 7.5 mm at u_0 = 6 m/s, Re_H = 2660)

RESULTS

Spatio-Temporal Distribution

Figure 4 shows an example of instantaneous distributions of temperature on the titanium foil as measured using infrared thermograph (FS, H = 7.5 mm, u_0 = 6 m/s). Bad pixels existed in the thermo-images were removed by applying a 3×3 median filter (here, intermediate three values were averaged). In addition, a low-pass filter (sharp cut-off) was applied in order to remove a high frequency noise more than a cutoff frequency f_c and the small-scale spatial noise less than a cutoff wavelength b_c (The values of f_c and b_c are listed in Table 1).

Figure 5 shows power spectrums for both signal and noise of the temperature detected by the infrared thermograph for the close-up measurement, corresponding to Fig. 4 (b). The noise was estimated by measuring the steady temperature on the titanium foil glued on a copper plate. By applying the median and the low-pass filters, the noise was much reduced by about 10 dB, resulting that the S/N ratio of the measurement was greater than 1000 for f < 30 Hz and nearly 10 at the maximum frequency of f_c = 250 Hz.

Incidentally, the frequency response and spatial resolution of the measurement using infrared thermography and heated-thin-foil was investigated analytically (Nakamura [6]). It was reported that the upper limit of the detectable fluctuating frequency against noise, f_{max}, and the lower limit of the detectable spatial wavelength against noise, b_{min}, can be determined as a function of $\Delta h(\overline{T_w} - T_0)/\Delta T_{IR0}$ if thermophysical properties of the foil is specified (Δh can be defined as h_{rms} if ΔT_{IR0} is defined as rms value). These values in the reattachment region (FS, H = 7.5 mm, u_0 = 6 m/s) were f_{max} = 157 Hz and b_{min} = 0.5 mm (Δh = 20 W/m^{2}K, $\overline{T_w} - T_0$ = 20^{o}C, ΔT_{IR0} = 0.018^{o}C, for a 2 μm thick titanium foil). Although the cutoff frequency f_c = 250 Hz (see Table 1) was greater than f_{max}, the measurement was possible since the noise was much reduced by applying the median and the low-pass filters, as shown in Fig. 5.

The local and instantaneous heat transfer coefficient was calculated using the following equation derived from the heat conduction equation in a thin foil.

$$h = \frac{\dot{q}_{in} - \dot{q}_{cd} - \dot{q}_{rd} - \dot{q}_{rdi} + \lambda\delta\left(\frac{\partial^2 T_w}{\partial x^2} + \frac{\partial^2 T_w}{\partial z^2}\right) - c\rho\delta\frac{\partial T_w}{\partial t}}{T_w - T_0} \qquad (2)$$

$\dot{q}_{in}$ is the input heat-flux to the titanium foil, $\dot{q}_{cd}$ is heat conduction to the air layer inside the test plate, $\dot{q}_{rd}$ and $\dot{q}_{rdi}$ are radiation heat fluxes to outside and inside the test plate, respectively.

This equation contains both terms of lateral conduction through the foil, $\lambda\delta$ ($\partial^2 T_w/\partial x^2 + \partial^2 T_w/\partial z^2$), and the delay due to the heat capacity of the foil, $c\rho\delta$($\partial T_w/\partial t$). Heat conduction to the air layer inside the wall, $\dot{q}_{cd} = -\lambda_a (\partial T/\partial y)_{y=0-}$ in Eq. (2), was calculated using the temperature distribution in the air layer, which can be determined by solving the heat conduction equation as follows (coordinate system is shown in Fig. 1).

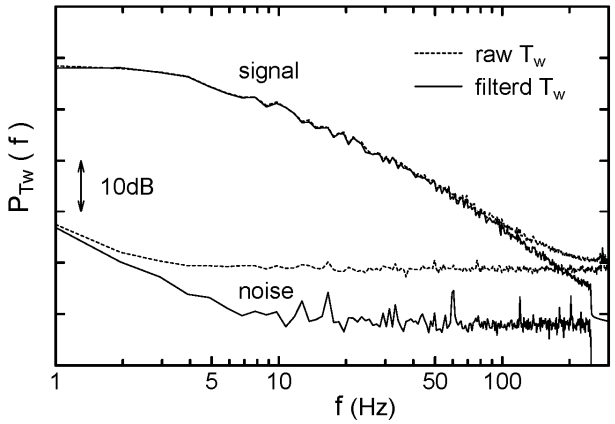

FIGURE 5. POWER SPECTRUM OF THE TEMPERATURE FLUCTUATION: signal – temperature for FS (u_0 = 6 m/s) at the reattaching region; noise – temperature on a steady temperature plate.

$$c_a\rho_a\frac{\partial T}{\partial t} = \lambda_a\left(\frac{\partial^2 T}{\partial x^2} + \frac{\partial^2 T}{\partial y^2} + \frac{\partial^2 T}{\partial z^2}\right), \quad (-\delta_a < y < 0) \qquad (3)$$

Since the temperature of the copper plate inside the test plate is assumed to be steady and uniform, the boundary condition of Eq. (3) on the copper plate side ($y = -\delta_a$) can be assumed as a mean temperature of the copper plate measured using thermocouples.

The finite difference method was applied to calculate the heat transfer coefficient h from Eq. (2) and (3). Time differential Δt corresponded to the frame interval of the thermo-images. Space differentials Δx and Δz corresponded to the pixel pitch of the thermo-image (for the condition of Fig. 4 (b), Δt = 1.0 ms and $\Delta x \approx \Delta z \approx$ 0.37 mm). The thickness of the air layer (δ_a = 1 mm) was divided into four or five regions (Δy = 0.25 mm for the wide measurements and 0.2 mm for the close-up measurements). Eq. (3) was solved using ADI (alternative direction implicit) method (Peaceman and Rachford [10]) with respect to x and z directions.

Figure 6 shows a cumulative power spectrum of the fluctuation of the heat transfer coefficient in the flow reattaching region measured using a high-speed heat flux sensor (HFM-7E/L, Vatell) under a condition of steady wall temperature (its power spectrum is shown later in Fig. 16). The time-constant of the sensor was faster than 3 kHz [11], which is sufficiently high to measure the fluctuation for the present conditions. Although the thermal boundary condition for the IR measurement was different from that for the HFS measurement

(uniform wall temperature), the cumulative power spectrum of both the measurements was considered to be similar because the power spectrum was similar (see Fig. 16). As indicated in Fig. 6 (a) and (b), the most part of the fluctuating energy (more than 95 % at the highest velocity of u_0 = 6 m/s) was included below the cutoff frequency of f_c.

The spatio-temporal distribution of the heat transfer coefficient corresponding to Fig. 4 (b), which was restored using the above procedure, is shown in Fig. 8. Also, the distribution for BS (H = 10 mm, u_0 = 6 m/s) and for BP (H = 3 mm, u_0 = 6 m/s) are respectively shown in Fig. 7 and 9. These figures reveal some unique characteristics of time-spatial behavior of the heat transfer for the separated and reattaching flow, which has hardly been clarified so far. The impressive

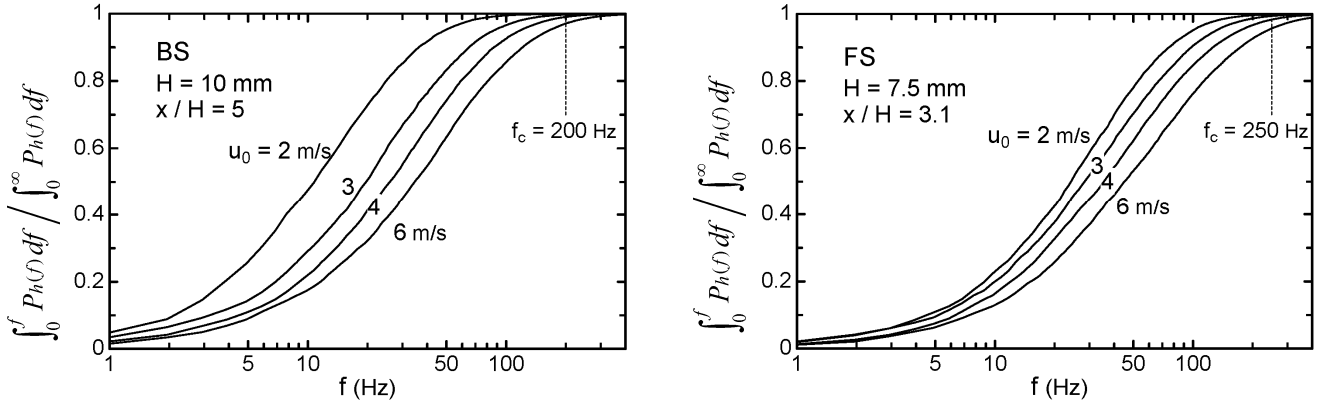

(a) BS (H = 10 mm, x = 50 mm) (b) FS (H = 7.5 mm, x = 23 mm)

FIGURE 6. COMULATIVE POWER SPECTRUM OF FLUCTUATING HEAT TRANSFER COEFFICIENT IN THE FLOW REATTACHING REGION MEASURED USING HIGH-SPEED HEAT FLUX SENSOR.

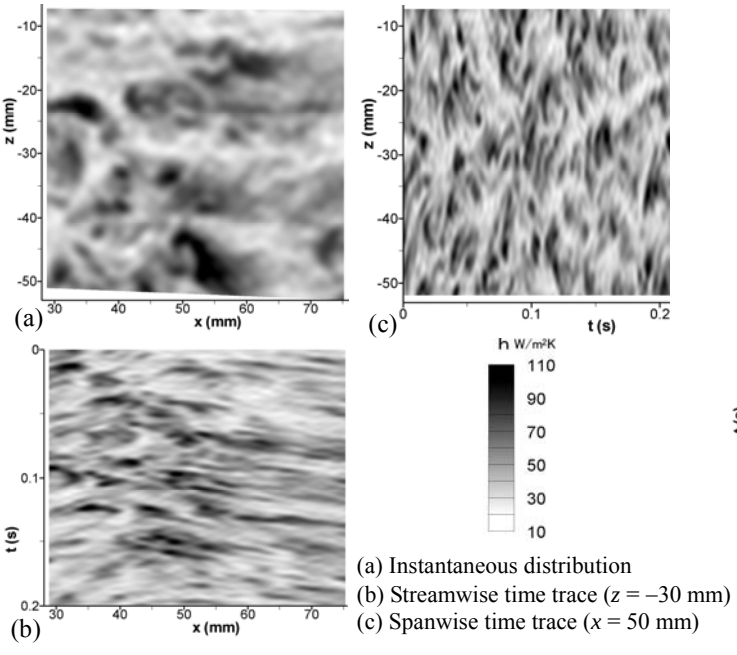

(a) Instantaneous distribution
(b) Streamwise time trace (z = –30 mm)
(c) Spanwise time trace (x = 50 mm)

FIGURE 7. TIME-SPATIAL DISTRIBUTION OF HEAT TRANSFER COEFFICIENT IN THE REATTACHING REGION
(BS: H = 10 mm at u_0 = 6 m/s, Re_H = 3560; close-up measurement; f_c = 200 Hz, b_c = 2.4 mm)

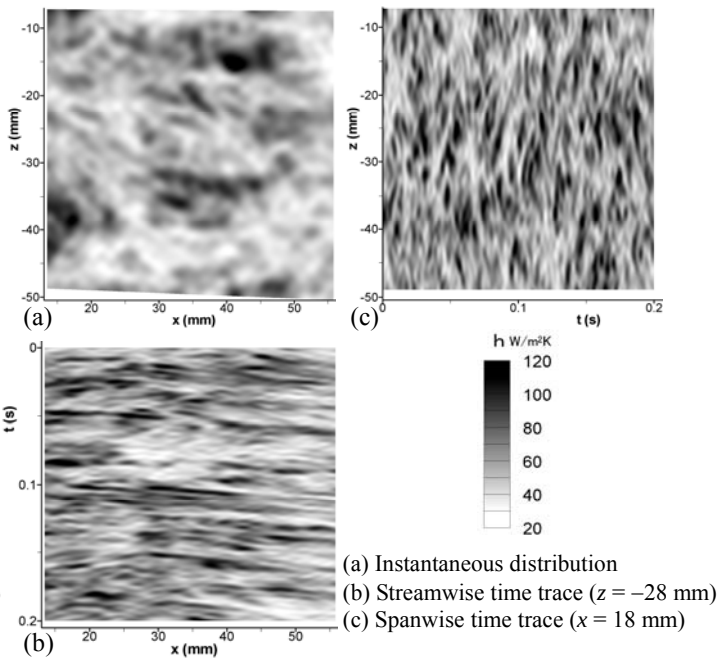

(a) Instantaneous distribution
(b) Streamwise time trace (z = –28 mm)
(c) Spanwise time trace (x = 18 mm)

FIGURE 8. TIME-SPATIAL DISTRIBUTION OF HEAT TRANSFER COEFFICIENT IN THE REATTACHING REGION (corresponding to Fig. 4 (b): FS: H = 7.5 mm at u_0 = 6 m/s, Re_H = 2660; close-up measurement; f_c = 250 Hz, b_c = 2.2 mm)

feature which is considered to be intrinsic in these flows is as follows: the heat transfer enhancement in the reattaching region ($x \approx 30 – 60$ mm for Fig. 7, $x \approx 10 – 50$ mm for Fig. 8, and $x = 10 – 40$ mm for Fig. 9) consists of a spot-like feature as shown in the instantaneous distributions (Fig. 7 – 9 (a)). The high heat transfer spots appear and disappear almost randomly but have some periodicity in time and spanwise direction, as indicated in the time traces (Fig. 7 – 9 (b), (c)). Each spot spreads with time, which forms a track of "∧" shape in the streamwise time trace (Fig. 7 – 9 (b)) corresponding to the streamwise spreading, and forms a track of "〈" shape in the spanwise time trace (Fig. 7 – 9 (c)) corresponding to the spanwise spreading. The basic behavior of the spot spreading overlaps with others to form a complex feature in terms of spatio-temporal characteristics of the heat transfer.

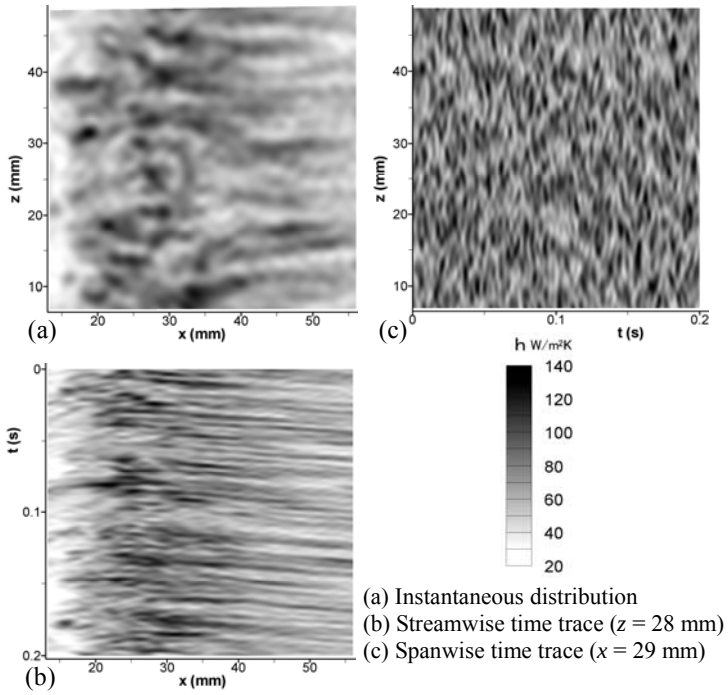

(a) Instantaneous distribution
(b) Streamwise time trace ($z = 28$ mm)
(c) Spanwise time trace ($x = 29$ mm)

FIGURE 9. TIME-SPATIAL DISTRIBUTION OF HEAT TRANSFER COEFFICIENT IN THE REATTACHING REGION
(BP: $H = 3$ mm at $u_0 = 6$ m/s, $Re_H = 1050$; close-up measurement; $f_c = 250$ Hz, $b_c = 2.2$ mm)

Time-Averaged Characteristics

In order to explore the similarity and dissimilarity in the heat transfer characteristics for the flow fields of BS, FS, and BP, the mean (time and span-averaged) characteristics are firstly investigated. Figure 10 shows the streamwise distributions of the mean heat transfer coefficient $\bar{h}$, which was calculated from the time-space distribution. The x axis is originated from the flow separation point. In each flow field, the heat transfer coefficient reaches a maximum by the flow reattachment (it was not confirmed at present whether the mean reattachment point coincides to the position of maximum $\bar{h}$), and it gradually decreases in the streamwise direction with a development toward a turbulent boundary layer flow.

Figure 11 shows streamwise distribution of Nusselt number, $Nu_H = \bar{h}H/\lambda$. Here, the Nusselt number was normalized by $Re_H^{2/3}$ because the local Nusselt number for the separated and reattaching flows usually proportional to $Re^{2/3}$ according to Richardson [12] and Igarashi [13]. As shown in Fig. 11, the distributions of $Nu_H/Re_H^{2/3}$ for each flow configuration (BS, FS, BP) tend to concentrate into a single curve in the region downstream of the flow reattachment region. It is remarkable that the Nusselt number distributions

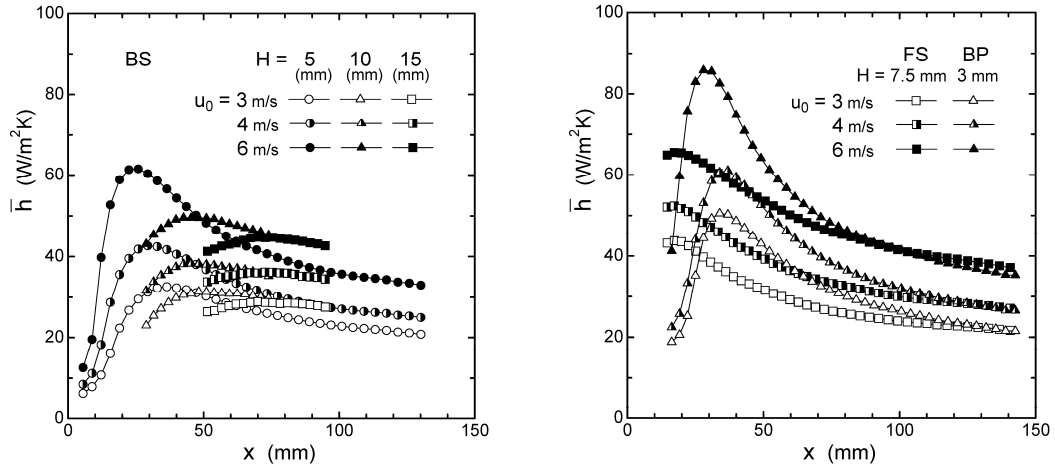

(a) BS (b) FS and BP

FIGURE 10. STREAMWISE DISTRIBUTION OF MEAN HEAT TRANSFER COEFFICIENT

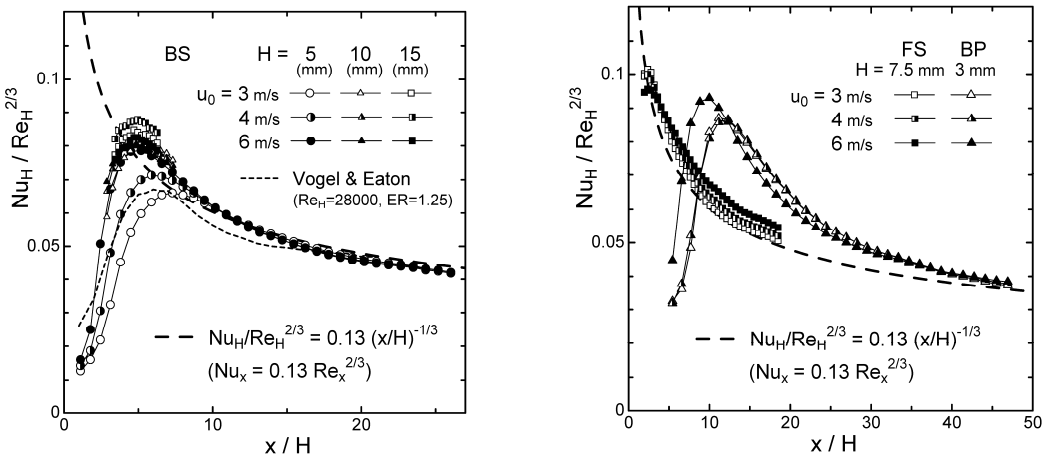

(a) BS (b) FS and BP

FIGURE 11. STREAMWISE DISTRIBUTION OF MEAN NUSSELT NUMBER

for BS and FS for downstream of the reattachment region can be approximated by the same relation as

$$Nu_H/Re_H^{2/3} = 0.13(x/H)^{-1/3} \quad (4)$$

Eq. (4) reduces to the following equation regardless of H

$$Nu_x = 0.13\ Re_x^{2/3} \quad (5)$$

Namely, the value of $Nu_x/Re_x^{2/3}$ behind the reattachment point can be approximated by a constant value of 0.13. The reason for this correspondence between BS and FS is not clear, but it may be related to the boundary layer thickness (δ_{99} = 24 – 28 mm) just upstream of the step, which is thicker than the step height.

The trend for BS (Fig. 11 (a)) fairly agrees to the previous investigation (Vogel and Eaton [1], among others) although the peak location somewhat differs ($x/H \approx 5$ for the present experiment for $Re_H \geq 2000$ and $x/H \approx 6$ for Vogel and Eaton at Re_H = 28000). The difference in the peak location can be explained by the fact that it moves downstream with an increase in the expansion ratio (ER), according to Durst and Tropea [14]. Also, it moves upstream with an increase in the turbulent boundary layer thickness upstream of the step (Eaton and Johnston [15]).

The Nusselt number for BP in the reattachment region is considerably higher than Eq. (4) and (5), as shown in Fig. 11 (b). This may be related to the thinner momentum thickness of the separated shear layer due to the uniform flow upstream of the blunt edge, the evidence of which is not clear at present.

As indicated in Fig. 11, the peak location in the Nu_H distribution shifts to downstream with a decrease in the freestream velocity. This trend is summarized in Fig. 12 as a variation of the peak location x_R', which indicates the separation length. The value of x_R'/H for BS is nearly constant for $Re_H \geq 2000$, however, it increases markedly for the lower Reynolds number (Re_H < 2000) with an elongation of the separation region.

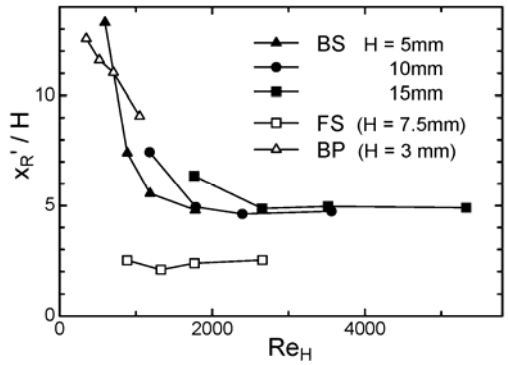

FIGURE 12. TREND OF PEAK LOCATION IN THE HEAT TRANSFER AGAINST REYNOLDS NUMBER

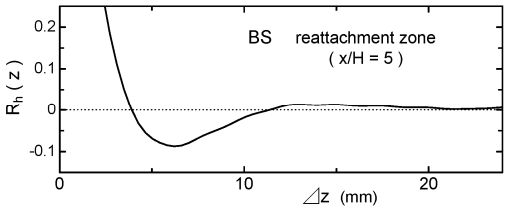

FIGURE 13. AUTOCORRELATION FUNCTION OF THE INSTANTANEOUS SPANWISE DISTRIBUTION (BS, H = 10 mm, u_0 = 6 m/s, x/H = 5)

Spatio Characteristics

As depicted in the spanwise time trace (Fig. 7 – 9 (c)), there seems to exist some spanwise periodicity in the heat transfer. Figure 13 shows an example of autocorrelation function of the instantaneous spanwise distribution at the reattaching region, which is averaged in time. The autocorrelation function for all conditions examined herein had a clear minimum, at Δz = 6.2 mm in the case of Fig 13. This minimum corresponds to a half wavelength $l_z/2$, thus, the typical spanwise wavelength can be defined as $l_z = 2\Delta z$. The values of l_z/H estimated here are plotted in Fig. 14 (a) against Reynolds number Re_H. It is remarkable that all plots for BS are almost concentrated into a single curve regardless of the step height H. In particular, the wavelength l_z/H is almost constant of about 1.2 for $Re_H \geq 2000$, for which the separation length (x_R'/H) is nearly constant. The measurement performed by Kawamura et al. [3] using heat flux sensors also indicated that there is a spanwise periodicity of about 1.2H around the reattaching region behind a backward-facing step at the higher Reynolds number of Re_H = 19600.

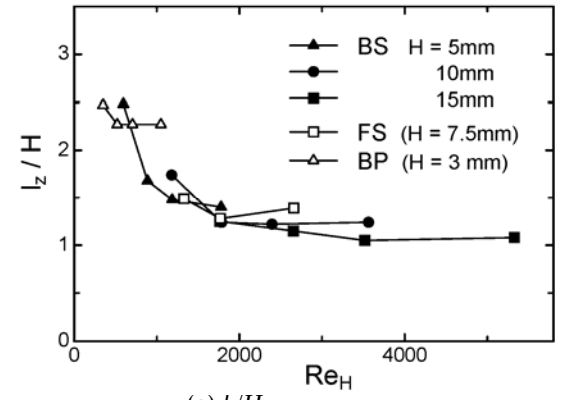

(a) l_z/H

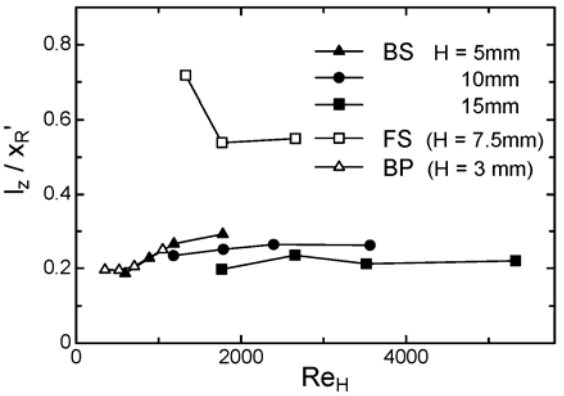

(b) l_z/x_R'

FIGURE 14. MEAN SPANWISE WAVELENGTH AT THE REATTACHING REGION AGAINST REYNOLDS NUMBER

Figure 14 (b) shows the trend of l_z normalized by the separation length (x_R'). Interestingly, the value of l_z/x_R' for BS is nearly constant (0.2 – 0.3) regardless of Re_H. This means that the typical spanwise wavelength for BS is roughly one-fourth of the separation length. From the result obtained here, it can be suggested that the origin of the spanwise periodicity is not the instability upstream of the flow separation (i.e. mean spanwise wavelength of the turbulent boundary layer upstream of the step), but due to some instability after the separation, which is dominated by the dimension of the separation region.

The trends for FS and BP are not clear at present since the data for these configurations are not sufficient to evaluate. But there seems to exist a typical spanwise wavelength; l_z/H = 1.2 – 1.5 for FS, and l_z/H = 2.2 – 2.5 for BP. The additional experiments are necessary to discuss this further.

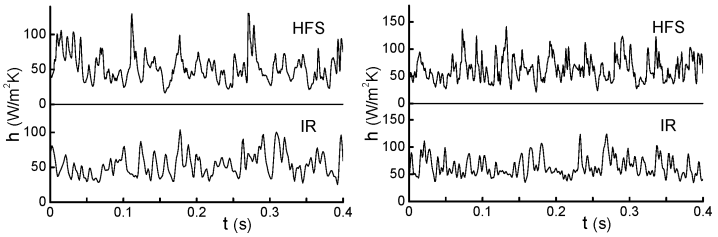

(a) BS (H = 10 mm, u_0 = 6 m/s, x/H = 5)

(b) FS (H = 7.5 mm, u_0 = 6 m/s, x/H = 3.1)

FIGURE 15. TIME TRACE OF THE HEAT TRANSFER COEFFICIENT top – HFS measurement; bottom – IR measurement

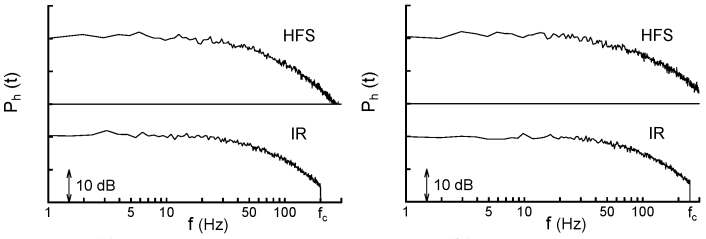

(a) BS (b) FS

FIGURE 16. POWER SPECTRUM OF THE FLUCTUATING HEAT TRANSFER COEFFICIENT CORRESPONDING TO FIG.15

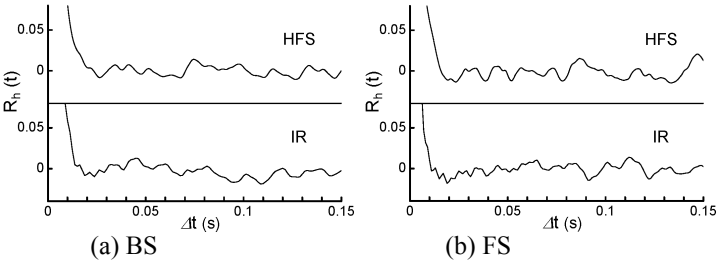

(a) BS (b) FS

FIGURE 17. AUTOCORRELATION OF THE FLUCTUATING HEAT TRANSFER COEFFICIENT CORRESPONDING TO FIG.15

Temporal Characteristics

Figure 15 shows time traces of the fluctuating heat transfer coefficient in the reattaching region measured using the heat flux sensor (HFS) and the infrared thermograph (IR). Although the time trace of IR does not have sharp peaks as that of HFS due to the low-pass filter at f_c, the basic characteristics seems to be similar. This validated the reliability of the fluctuating heat transfer restored based on the IR measurement.

Figure 16 shows power spectrum of the fluctuation corresponding to Fig. 15. The trend of the power spectrum which attenuates with frequency is similar between for IR and HFS up to the sharp-cutoff frequency f_c, although the thermal boundary condition is different. This indicates that the characteristics of the fluctuating heat transfer seem to be independent to the thermal boundary condition, but dominated by the flow field (vortical structure) near the wall.

The previous studies have indicated that the flow in the reattaching region behind a backward-facing step was dominated by "the low-frequency unsteadiness". Eaton and Johnston [16] measured the energy spectra of the streamwise velocity fluctuations at several locations and reported that the spectral peak occurred at the Strouhal number of $St_H = fH/u_0 = 0.066 – 0.08$. The direct numerical simulation performed by Le et al. [17] also showed that the dominant frequency of velocities was roughly $St_H = 0.06$. The origin of this unsteadiness is not yet completely understood, but it may be caused by the pairing of the shear layer vortices, according to Schäfer et al. [18].

In order to investigate whether the heat transfer also has the temporal periodicity reflected by "the low frequency unsteadiness", an autocorrelation function of the fluctuating heat transfer was calculated. The results corresponding to Fig. 15 are shown in Fig. 17. Although there was no clear periodicity in the power spectrum, as shown in Fig. 16, the autocorrelation have quasi-periodic bumps, indicating that there is some characteristic period in the fluctuation.

Then, a typical period Δt was estimated from the autocorrelation in the similar manner to the spanwise wavelength, i.e., the period to the first minimum was defined as $\Delta t/2$. Since the first minimum was not clear compared to that for the spanwise wavelength (see Fig. 13), the value Δt could not always be estimated here, and therefore, Δt was estimated only for the cases for which the first minimum was easily distinguished.

The Strouhal numbers estimated from the HFS data, $St_H = fH/u_0$, are plotted in Fig. 18 against the streamwise position x/x_R'. The typical fluctuating frequency f was defined as $1/\Delta t$. For BS (Fig. 18 (a)), the Strouhal number behind the reattaching region ($x/x_R' = 1 – 3$) tends to concentrate in a specific range of $St_H = 0.05 – 0.1$, regardless of the experimental conditions such as step height and freestream velocity. Despite the value has a considerable scatter, the frequency of $St_H = 0.05 – 0.1$ seems to be similar to that of "the low frequency unsteadiness", which has been widely observed in the flow field [16, 17, among others]. Namely, it is

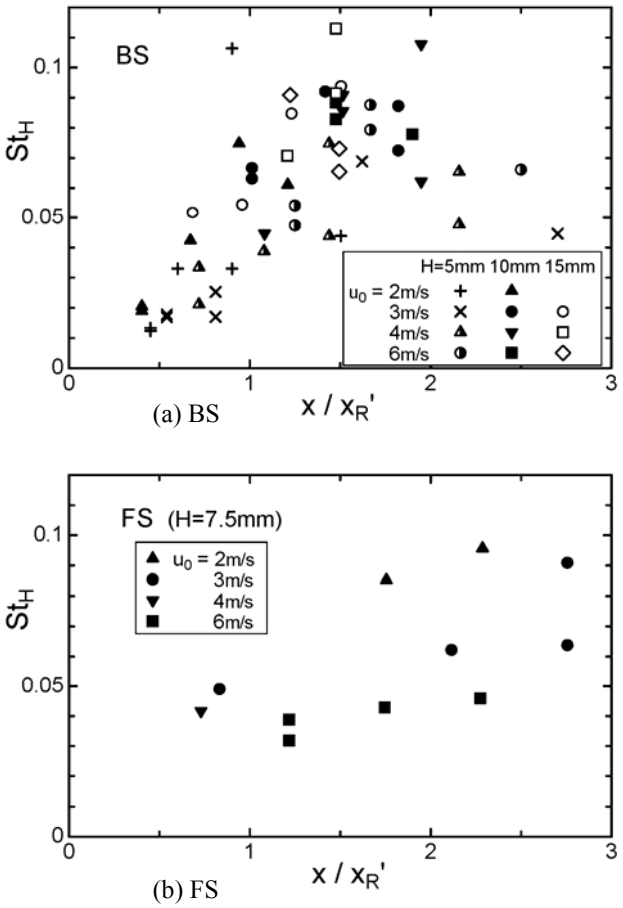

FIGURE 18. STROUHAL NUMBER ESTIMATED FROM AUTOCORRELATION OF THE FLUCTUATING HEAT TANSFER COEFFICIENT MEASURED USING HEAT FLUX SENSOR

reasonable to suppose that the heat transfer in the reattaching region has temporal characteristics reflected by the low frequency unsteadiness in the flow field.

For FS (Fig. 18 (b)), the Strouhal number behind the reattaching region ($x/x_R' = 1.5 – 3$) also has values in a specific range of $St_H = 0.04 – 0.1$, which is similar to that for BS. This suggests that the temporal characteristics for both BS and FS are related to the dimension of the separation region (characteristic length H or separation length x_R), as well as the spanwise wavelength.

If the spatio-temporal characteristics behind the reattaching region originate from the streak structure in the turbulent boundary layer upstream of the step, its spanwise wavelength and typical period ought to decrease with the freestream velocity regardless of the step height H. This indicates that the spatio-temporal characteristics around the reattaching region are not due to the instability before the flow separation, but due to some instability, which is accompanied by the flow separation and reattachment. Further study is necessary to

explore the origin of the spanwise and temporal periodicities observed in this work.

CONCLUSIONS

The spatio-temporal distribution of heat transfer behind a backward-facing step (BS), behind a forward-facing step (FS), and on a blunt plate (BP), were examined by employing a technique using high-speed infrared thermograph.

It was possible to restore the heat transfer coefficient in the flow reattaching region up to 250 Hz in time and up to 2.2 mm in space by employing a 2 μm thick titanium foil as a heated thin-foil. This frequency range covered most of the fluctuating energy of the heat transfer, and thus, the quantitative distribution can be restored, which was reflected by the turbulent vortical structure near the wall.

The measurements revealed that the heat transfer in the flow reattaching region had spot-like characteristics. The each spot of high heat transfer spread with time and overlapped with others to form a complex feature in terms of spatio-temporal characteristics.

The mean Nusselt number distribution behind the reattaching region was approximately proportional to 2/3 power of Reynolds number, as indicated in the previous researches. It was remarkable that the distribution of $Nu_x/Re_x^{2/3}$ for BS and FS tended to concentrate into a constant value regardless of the experimental conditions.

In the time-space distribution of the heat transfer, there was a typical spanwise wavelength and a typical fluctuating frequency in the reattaching region, both of which was likely to be related to the dimension of the separation region (characteristic length H or the separation length x_R). In particular, for BS, the typical wavelength normalized by the separation length was nearly constant (l_z/x_R' = 0.2 – 0.3) regardless of the experimental conditions. (Here, x_R' was defined by the position where the heat transfer coefficient reached maximum.) This indicates that the origin of the spanwise periodicity is not the instability upstream of the flow separation, but due to some instability, which is accompanied by the flow separation and reattachment.

For BS and FS, the typical frequency of the fluctuating heat transfer behind the reattaching region was $St_H = fH/u_0$ = 0.05 – 0.1, although there was a considerable scatter. This fluctuation is likely to be related to the low-frequency unsteadiness in the flow field reported in previously published literature.

ACKNOWLEDGMENTS

This research was supported by a Grant-in-Aid for Scientific Research (#22560214), from the Japan Society for the Promotion of Science (JSPS). The author wishes to acknowledge to Mr. Akira Kodama and Mr. Yuya Yamaguchi, the former student of the National Defense Academy, Japan, for their assistance in the experiments and data analysis.

REFERENCES

[1] Vogel, J.C., and Eaton, J.K., 1985. “. Combined Heat Transfer and Fluid Dynamic Measurements Downstream of a Backward-Facing Step”. *Trans. ASME J. Heat Transfer*, **107**, pp. 922-929.

[2] Kawamura, T., Tanaka, S., Kumada, M., and Mabuchi, I., 1988. “ Time and Spatial Unsteady Characteristics of Heat Transfer at the Reattachment Region of a Backward-Facing Step” (in Japanese). *Transactions of Japan Society of Mechanical Engineers B*, **54**(504), pp.1224-1232.

[3] Kawamura, T., Yamamori, M., Mimatsu, J., and Kumada, M., 1994. “Three-Dimensional Unsteady Characteristics of Heat Transfer around Reattachment Region of Backward-Facing Step Flow” (in Japanese). *Transactions of Japan Society of Mechanical Engineers B*, **60**(576), pp.2833-2839.

[4] Hetsroni, G., Mosyal, A., and Yarin, P., 1997. “Thermal Streaks Regeneration in the Wake of a Disturbance in a Turbulent Boundary Layer”, *Int. J. Heat and Mass Transf.*, **40**, pp.4161-4168.

[5] Oyakawa, K., Miyagi, T., Oshiro, S., Senaha, I., Yaga, M., and Hiwada, M., 2000. “Study on Time-Spatial Characteristics of Heat Transfer by Visualization of Infrared Images and Dye Flow”, *Proceedings of 9th International Symposium on Flow Visualization*, Pap. no. 233.

[6] Nakamura, H., 2009. “Frequency-Response and Space-Resolution of a Thin Foil for Heat Transfer Measurements Using Infrared Thermograph”. *Int. J. Heat and Mass Transfer*, **52**, pp. 5040-5045.

[7] Nakamura, H., 2007. “Measurements of Time-Space Distribution of Convective Heat Transfer to Air Using a Thin Conductive-Film”. *5th Int. Symposium on Turbulence and Shear Flow Phenomena*, München, pp.773-778.

[8] Igarashi, T., Nakamura, H., and Morita, T., 2003. “Pressure Drop and Heat Transfer of a Rectangular Block on the Wall of Parallel Plates Channel (Effect of the Opening Ratio)”, *4th Int. Symp. on Turbulence, Heat and Mass Transfer*, Antalya, Turkey, pp.309-316.

[9] Pellow, A., and Southwell, R.V., 1940. “ On Maintained Convective Motion in a Fluid Heated from Below”. *Proceedings of the Royal Society A*, **175**, pp.312.

[10] Peaceman, D.W., and Rachford, H.H., 1955. “The numerical solution of parabolic and elliptic differential equations”. *J. Soc. Ind. Appl. Math.*, **3**, pp.28-41.

[11] Nakamura, H., and Igarashi, T., 2004. “Unsteady Heat Transfer from a Circular Cylinder for Reynolds Numbers from 3000 to 15000”, *Int. J. Heat and Fluid Flow*, **25**(5), pp.741-748

[12] Richardson, P.D., 1963. “Heat and Mass Transfer in Turbulent Separated Flows”. *Chemical Engineering Science*, **18**, pp. 149-155.

[13] Igarashi, T., 1986. “Local Heat Transfer from a Square Prism to an Air Stream”. *Int. J. Heat and Mass Transfer*, **29**(5), pp. 777-784.

[14] Durst, F., and Tropea, C., 1981. “Turbulent, Backward-Facing Step Flows in Two-Dimensional Ducts and

Channels". *Proc. 3rd Int. Symp. on Turbulent Shear Flows*, Davis, CA, pp.18.1-18.6.
[15] Eaton, J.K., and Johnston, J.P., 1981. "A Review of on Subsonic Turbulent Flow Reattachment". *AIAA J.*, **19**(9), pp. 1093-1100.
[16] Eaton, J.K., and Johnston, J.P., 1980. "Turbulent Flow Reattachment: An Experimental Study of the Flow and Structure behind a Backward-Facing Step". *Rep.*, MD-39, Thermosciences Division, Dept. of Mech. Engng, Stanford University.
[17] Le, H., Moin, P. and Kim, J., 1997. "Direct Numerical Simulation of Turbulent Flow Over a Backward-Facing Step". *J. Fluid Mech.*, **330**, pp.349-374.
[18] Schäfer, F., Breuer, M., and Durst, F., 2007. "The Dynamics of the Transitional Flow Over a Backward-Facing Step". *J. Fluid Mech.*, **623**, pp.85-119.